A&A 451, 909–916 (2006)
DOI: 10.1051/0004-6361:20054009
© ESO 2006

Astronomy & Astrophysics

Kinematic structure of the corona of the Ursa Major flow found using proper motions and radial velocities of single stars*

N. V. Chupina, V. G. Reva, and S. V. Vereshchagin

Institute of Astronomy of the Russian Academy of Sciences, 48 Pyatnitskaya Str., 119017 Moscow, Russia
e-mail: svv@inasan.ru

Received 8 August 2005 / Accepted 5 January 2006

ABSTRACT

Aims. We study the kinematic structure of peripheral areas of the Ursa Majoris stream (Sirius supercluster).
Methods. We use diagrams of individual stellar apexes developed by us and the classical technique of proper motion diagrams generalized to a star sample distributed over the sky.
Results. Out of 128 cluster members we have identified three corona (sub)structures comprised of 13, 13 and 8 stars. The substructures have a spatial extension comparable to the size of the corona. Kinematically, these groups are distinguished by their proper motions, radial velocities and by the directions of their spatial motion. Coordinates of their apexes significantly differ from those of the apexes of the stream and its nucleus. Our analysis shows that these substructures do not belong to known kinematic groups, such as Hyades or Castor. We find kinematic inhomogeneity of the corona of the UMa stream.

Key words. stars: formation – open clusters and associations: Ursa Major

1. Introduction

The estimates of mass and reliable measurements of the astrometric parameters of stars obtained with the Hipparcos satellite (HIP, ESA 1997) allow us to study the kinematic structure of stellar flows using the classical method of proper motion diagrams. This method allows us to find the radiant of the spatial motion of stars from proper motions considered in a special coordinate frame, the VA frame. This method was developed by van Altena (1969) for the investigation of the Hyades star stream. We apply proper motion diagrams to the Ursa Major star flow (Sirius supercluster). The flow contains two components: the nucleus, which is located around the Big Dipper and a corona, with stars scattered over the sky. We did not try to find new members of the stream. Rather, we study certain kinematic structures or substructures of the peripheral areas of the flow. In this work we use a sample of stars, compiled from published data, that differ both in the number of stars and in their membership probability.

The major feature in a moving group is the common value of space motion vectors of moving stars; other parameters are of secondary importance. To the astrometric parameters that became available from the Hipparcos catalogue, we have added radial velocities from the CDS catalogues. Detailed study of the proper motion diagram (PMD) of the stream and the diagram of the individual stellar apexes (AD, Chupina et al. 2001, Paper I) has allowed us to investigate the structure of the flow and to find the kinematic substructures inside its corona.

2. Observational data

To compile a list of members of the Ursa Majoris stream we used results of a number of published studies. Our list contains only single stars. The reason for this is the displacement of positions of double and multiple stars in the PMD due to the orbital motion of components. This problem requires a special analysis.

In Table 7 we present data taken from the HIP catalogues and Duflot et al. 1995 (CDS number 3190A), and proper motions calculated by us in the van Altena system and their rms-errors. Table 7 has sub-sections corresponding to the cluster core, corona, and to groups identified in this study. We also show separately the "possible non-members" of the above structures. Table 7 contains: stellar identification numbers in the HIP and HD catalogues and the astrometric parameters with their errors from HIP, proper motions in the equatorial coordinate system and parallaxes, components of proper motion in the van Altena reference frame and their rms deviations, the values of $\sin\lambda$ (the angle between directions to the apex and to the star). Table 7 contains data on 128 stars. For 121 stars we use radial velocities from Duflot et al. (1995); these velocities are also listed in Table 7.

The flags in the last six columns are 1 if the star belongs to the UMa flow or 0 otherwise, according to criteria accepted in the original publication. This status is related to the probability of the membership of the star. The distribution of the stars over the flags is given in Table 1. Approximately 20% of all stars are considered as members of the flow by more than three authors simultaneously. The numbers of stars taken from the quoted papers are:

- Roman (1949, Table 18), $n = 67$.
- Eggen (1959, Table 1), $n = 39$.
- Soderblom & Mayor (1993, Table 11), $n = 14$. It contains so-called probable members (the nucleus stars and some others selected both by spectral index and by kinematics) and possible members for which the kinematic data is located within a 3σ error ellipsoid.
- Eggen (1998, Table 1), $n = 17$.

* Table 7 is only available in electronic form at http://www.edpsciences.org

Article published by EDP Sciences and available at http://www.edpsciences.org/aa or http://dx.doi.org/10.1051/0004-6361:20054009

Table 1. Distribution of stars over flags. Designations: nflags – the number of flags equal to 1, nstars – the number of stars with this amount of flags equal to 1.

nflags	nstars
1	54
2	47
3	13
4	7
5	6
6	1

– Montes et al. (2001) (n = 39) present a compilation of stars with spectral classes later than F2 and data on several kinematic groups including the UMa stream.
  Only single stars are considered. They use kinematic and photometric parameters as membership criteria, as well as other constraints: level of chromospheric activity, rotation and lithium abundance. Precise astrometric data from the HIP and Tycho-2 catalogues are updated with radial velocities taken from various sources. We use 39 out of 84 stars of Montes et al. (2001). The difference is due to more rigid conditions constraining single stars in the present work. For example we classify a star as a single one if the H55 flag is set to "the star is not in the CCDM", it is not a multiple or a binary system according to flag H59, and has a "S" solution quality according to the H61 flag.
– King et al. (2003), n = 47. Using HIP astrometry and original radial velocities and new measurements of spectral emission indeces King et al. (2003) revised the membership status of some 220 stars. The final list of nearly 60 assumed members is used by us. In comparison to Paper I, we have considered an additional 34 stars from King et al. (2003). We considered only single stars. In the basic catalogue of King et al. (2003) no attributes of multiplicity or binarity are provided. However, we excluded three stars considered double according to the Notes in the basic catalogue (Table 3, see King et al. (2003)): HD 18645 and HD 129674 – spectroscopic binaries and HD 29697 a star that is variable probably due to its binarity.

The inverse Gaussian error distribution on the parallax is not Gaussian, and the expected value of the distance thus differs from the inverse of the parallax for high values of the relative errors. Stars HIP 7617, 36041, 36041 were excluded from the sample as having relatively poor parallaxes with errors exceeding 20%, see Table 7.

3. The AD diagram

Positions of individual stellar apexes in the equatorial coordinate system are shown in Fig. 1. The Figure represents the points on the celestial sphere where the vectors of stellar space velocity transferred to the observer's position pass through. Their coordinates are designated as A for right ascension and D for declination, by analogy with the usual apex. These points may be called "individual stellar apexes". The technique of construction of AD-diagrams, their formal description and the formulae for determination of the error ellipses are given in Paper I.

Three stars have remained outside the limits of the diagram. The data on these stars are given in Table 2. The A-values are outside the diagram by several tens of degrees. This occurs because these stars have distinctive components of space velocity; HIP 99913 due to its exceptionally high value of proper motion

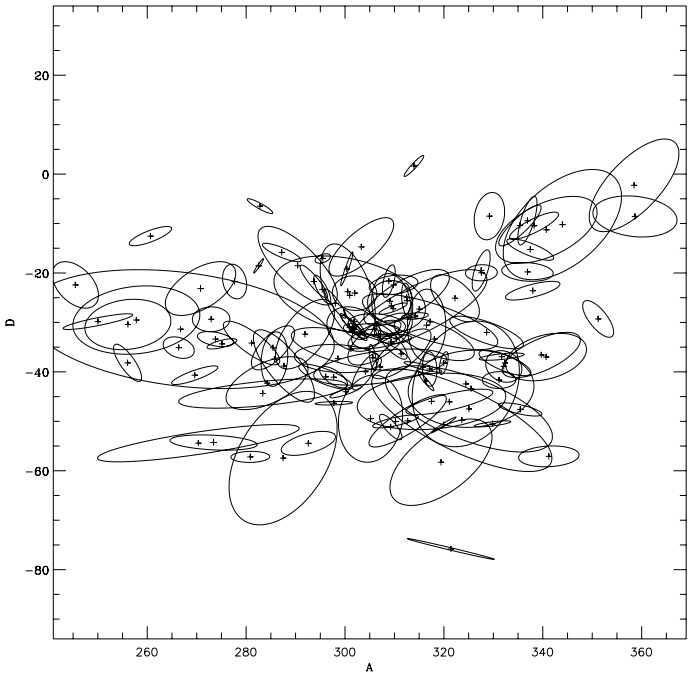

Fig. 1. The AD diagram of 116 stars with known radial velocities (2 stars with σ_π/π > 20% were excluded (see Table 7) and 3 stars appeared outside the diagram. The data are given in Table 2). Ellipses around the points characterize the errors of calculated A and D values.

and HIP 29716 due to excessive radial velocity. HIP 99913 is considered as a flow member by Roman (1949) only, HIP 29716 is considered as a member by King et al. (2003) only, HIP 21818 by Montes et al. (2001) only.

The main features of Fig. 1 are better seen in Figs. 2 and 3:

1) Fig. 2 shows the AD-diagram for the subsets of stars with the maximum point concentration in Fig. 1. The central diagonal line formed by 8 stars of the nucleus investigated in Paper I is seen. The large axes of the ellipses of errors are focused along the diagonal which may be drawn from the upper left corner of the diagram to the right bottom corner. The sizes of ellipse axes are small in comparison to other stars. The scatter of points along the diagonal is caused by the errors of radial velocity measurements (see Paper I) and the errors in the moduli of proper motion measurements. Other structures seen in Fig. 1 that are formed by large ellipse axes allow us to distinguish substructures inside the UMa flow, as seen in Fig. 2. Three stellar substructures seen in Fig. 1 are distinguished: group 1 in the right upper diagonal, group 2 to the left of the nucleus and group 3 that is located perpendicularly to the nucleus and is directed to the bottom of the diagram. The separate location of stellar groups in the AD-diagram (see Fig. 2) and the similar orientation of their ellipse axes provides evidence for the existence of their own apexes, as is seen from Table 3. In Table 3 we give apexes for the groups, calculated using formulae given in Paper I. The apex for the nucleus is given according to Paper I. Groups 1, 2 and 3 are distinguished both by point positions in the AD-diagram and by orientation and size of the ellipses of errors. The single rms-value of 0.3 km s^{-1} adopted by us for all sample stars shows the distribution of sizes and orientations of error ellipses in Fig. 1. Using individual errors would contaminate the ellipse distribution, making the figure less clear.
2) What are the reasons for the large differences in the ellipse size in Fig. 1? In Fig. 3 we show the AD-diagrams for stars

Table 2. The stars that are outside the AD-diagram in Fig.1. Catalog numbers and parameters are given.

HD	HIP	HR	A	D	μ_α	μ_δ	μ_U	μ_T	V_r	π	remarks
					mas/yr		mas/yr		km s^{-1}	mas	
29697	21818		27°.44	–27°.20	–233.61	–254.55	225.81	80.42	11.0	74.13	
43318	29716		58°.60	–38°.85	–158.04	–218.33	521.20	–43.46	38.1	28.02	μ_U and V_r are very large
192836	99913	7746	29°.38	–73°.48	8.10	–25.73	96.58	50.47	–4.1	10.95	

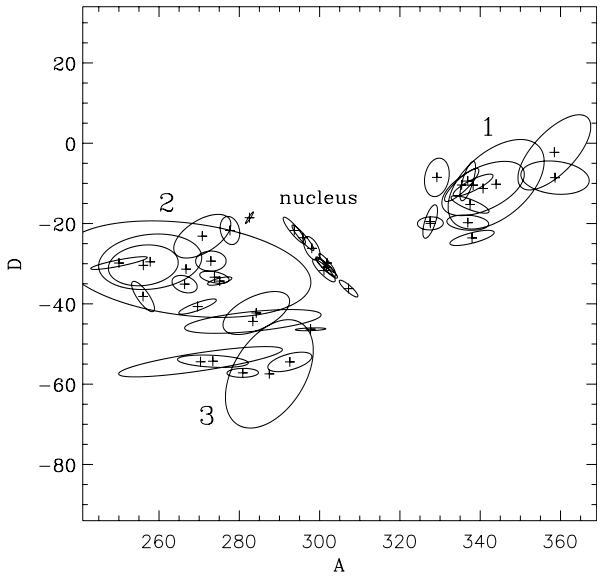

Fig. 2. The stars of the nucleus and of the groups representing different areas of the point concentration in the general diagram plane.

Table 3. Positions of the apexes for the groups and the nucleus.

group	A	D
1	341°.47	−12°.59
2	267°.34	−30°.43
3	283°.75	−51°.35
nucleus	300°.58	–29°.21

with different distances to the Sun. On average, the most distant stars have the largest sizes of the ellipse axes, because these sizes are nearly proportional to the inverse values of the parallaxes.

The vectors of spatial velocity used for the construction of AD-diagrams involve radial velocities and proper motion components. Thus, the sizes of the ellipse axes are influenced by the errors of proper motions, radial velocities and parallaxes. Parallaxes are used for transformation of proper motions into tangential velocities.

4. Radial velocities

Figure 4 shows the dependence of the V_r-velocity on the cosine of the angular distance of the star from the apex of the UMa flow ($\cos\lambda$). For the top panel the apex for UMa flow was used, for the bottom panel the apexes of separate groups were used. On average, the dependence is linear. For some stars large deviations exist, both for stars belonging to different groups and to the nucleus.

The dotted line shown in Fig. 4 was constructed from Fig. 5 that shows components of the stellar velocity vector ($\boldsymbol{V}$) directed to the apex K. The origin of $\boldsymbol{V}_r$ is at the point of the stellar position on the great circle of the celestial sphere. If the star belongs to the flow moving with a constant velocity V, the $V_r - \cos\lambda$ dependence will be a straight line according to the formula $V_r = V\cos\lambda$. We see this in Fig. 4 (left panel): the points are located close to the straight line $V_r = 20\cos\lambda$ (a mean flow space velocity $V = 20$ km s^{-1} is used).

In Table 4 we present some statistics for groups, corona and the nucleus from Fig. 4. This Table gives the number of stars n, $|\Delta V_{r1}|$ the average deviation from the line $V_r = 20\cos\lambda$, $|\Delta V_{r2}|$, the average deviation from the straight line computed for individual groups with their intrinsic apexes. The ratio $\frac{|\Delta V_{r1}|}{|\Delta V_{r2}|}$ shows that transition to group apexes had the most influence for groups 1 and 2. This means that the motion of these groups differs most from the mean motion of flow.

In Fig. 4:

1) With the transition to individual group apexes taken from Table 4, the scatter of points of groups 1–3 considerably decreases, see $\frac{|\Delta V_{r1}|}{|\Delta V_{r2}|}$-coefficients from Table 4.
2) The stars of group 1 are spread over the whole interval of $\cos\lambda$. Thus, group 1 includes the stars with angular distances between apex and antapex.
   The celestial sphere is divided in two by the great circle with poles at apex and antapex. The large circle with poles at the apex and antapex of the UMa stream divides the celestial sphere into two hemispheres: PA and PaA. The stars are located in both hemispheres and have deviations of radial velocities that are within the range $|\Delta V_r| \leq 9$ km s^{-1}. Such deviations of radial velocities from the straight line provide evidence for a difference of the intrinsic group apex from the UMa one.
3) 9 out of 13 stars group 2 stars are located in the PaA hemisphere (under the dotted line in Fig. 4 bottom). Their radial velocities differ from the average by less than 10 km s^{-1}.
4) 5 stars of group 3 are located above the straight line (in the PA hemisphere). Radial velocities of the majority of them are greater than the average. The average deviation of group 3 did not change at the transition to its own apex, see Table 4. This suggests apex uncertainty, and calls into doubt the existence of group 3.

5. Proper motion diagram

The proper motion diagram (PMD) is shown in Fig. 6 for all stars from Table 7. The μ_U axis is directed to the apex of the flow with coordinates $A_{UMa} = 303°.1$, $D_{UMa} = -34°.9$ calculated by weighting ($A = \Sigma A_i\pi_i/\Sigma\pi_i$) the average of points in the AD-diagram (Fig. 1). The coordinates in the figures are normalised to the geometrical center of the nucleus ($\lambda_c = 134°.86$) and to the average distance of the nucleus stars from the Sun ($R_c = 20$ pc).

In Fig. 7 the PMD for groups are shown in two cases: with a common apex (left) and with individual group apexes (right) from Table 3. In the latter case the axis μ_U is directed to the apex point of each group individually, with values taken from Table 3.

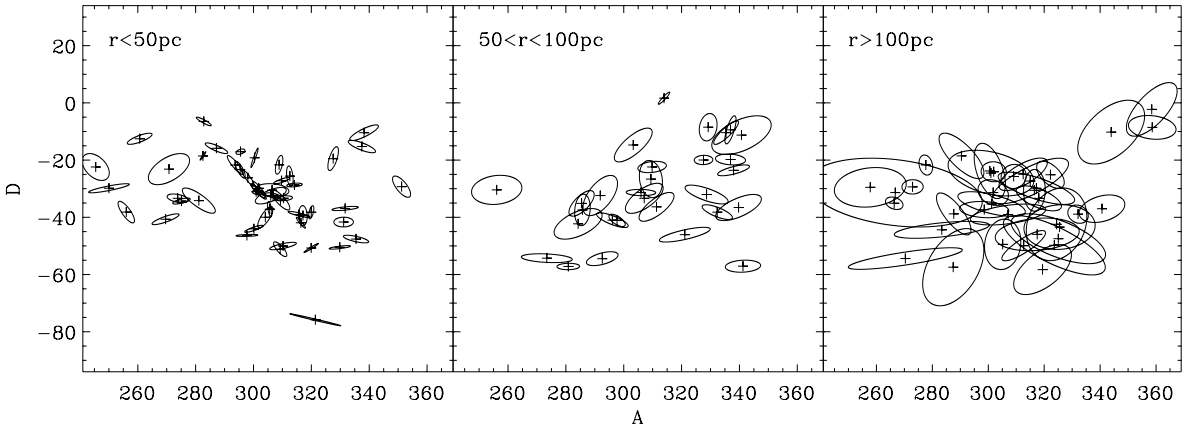

Fig. 3. The AD-diagrams for the stars located in the different intervals of distances from the Sun.

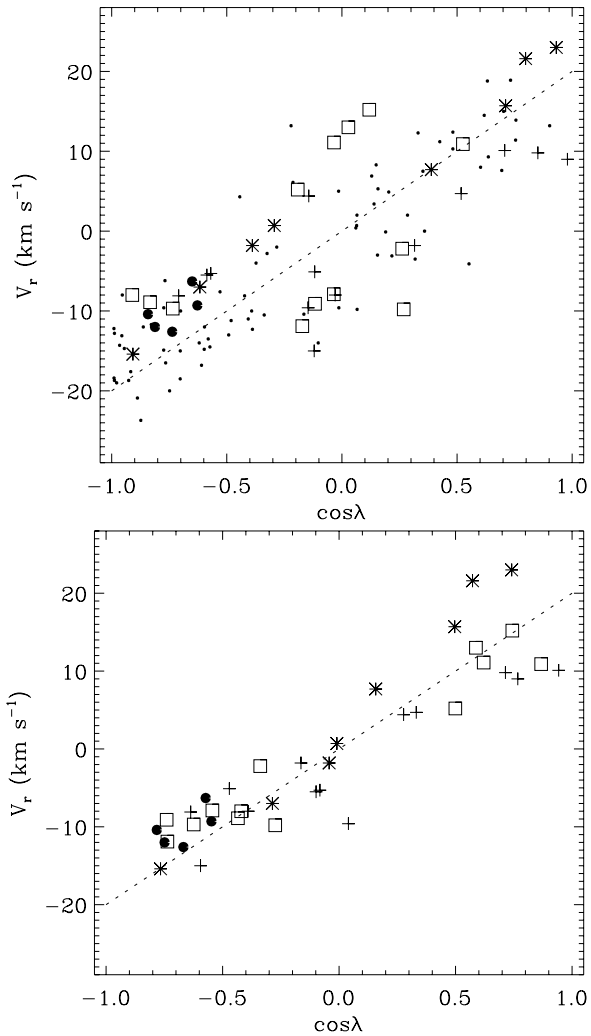

Fig. 4. Dependence of the radial velocity (V_r) on the cosine of the star angular distance from the apex position($\cos\lambda$). For the top panel the common apex for UMa flow was used, for the bottom panel the apexes of separate groups were used. The average dependence is shown with a dotted line. Squares represent the stars of group 1, crosses group 2, asterisks group 3, and filled circles the nucleus.

Coordinates in this frame are determined by:

$$\begin{aligned} \mu_{\rm U} &= \mu'_{\rm U}\frac{\sin\lambda_{\rm c}}{\sin\lambda}\frac{R}{R_{\rm c}} \\ \mu_{\rm T} &= \mu'_{\rm T}\frac{R}{R_{\rm c}}, \end{aligned} \tag{1}$$

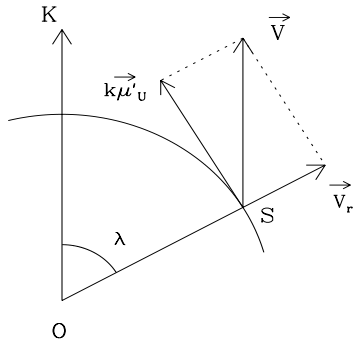

Fig. 5. Components of the stellar space velocity vector for a star moving to the apex K (k is the coefficient transforming $\mu'_{\rm U}$ from an angular to a linear scale).

Table 4. Statistical data on the $V_r - \cos\lambda$ dependence in Fig. 4. For computation of $|\Delta V_{r1}|$ the apex for UMa flow was used, while for $|\Delta V_{r2}|$ the individual group apexes were used.

group	n	$\lvert\Delta V_{r1}\rvert$	$\lvert\Delta V_{r2}\rvert$	$\frac{\lvert\Delta V_{r1}\rvert}{\lvert\Delta V_{r2}\rvert}$
1	13	8.8	2.9	3.0
2	13	7.0	4.1	1.7
3	8	4.0	4.0	1.0
corona stars	79	5.0	5.0	1.0
nucleus	5	4.6	3.2	1.4

where $\mu'_{\rm U}$ and $\mu'_{\rm T}$ are the proper motion components obtained by transformation of the usual components to the VA-system. The multiplier $\sin\lambda_{\rm c}/\sin\lambda$ is used for normalisation of $\mu_{\rm U}$-components by cancellation of the dependence of their sizes on the angular distance from the apex.

With the help of the PMD presented in Fig. 6 it is possible to test whether stellar motions in space are parallel: the $\mu_{\rm T}$-component should be close to zero for parallel stellar space velocities. The size of the $\mu_{\rm U}$-component for stream stars should coincide within the errors (for instance, $3\sigma_{\mu_{\rm U}}$).

Comparison of the left and right panels of Fig. 7 shows that the scatter of points has considerably decreased; this is confirmed by the mean deviations given in Table 5. The points of groups concentrate around $\mu_{\rm T} \approx 0$. In Table 5 the mean value of $\mu_{\rm T}$ and its rms for groups are given. Mean values deviate from zero for the UMa stream apex and become closer to it with transition to their own apex.

The kinematic picture will be complete if in addition to the already considered $\mu_{\rm T}$- and V_r-components of star velocity we

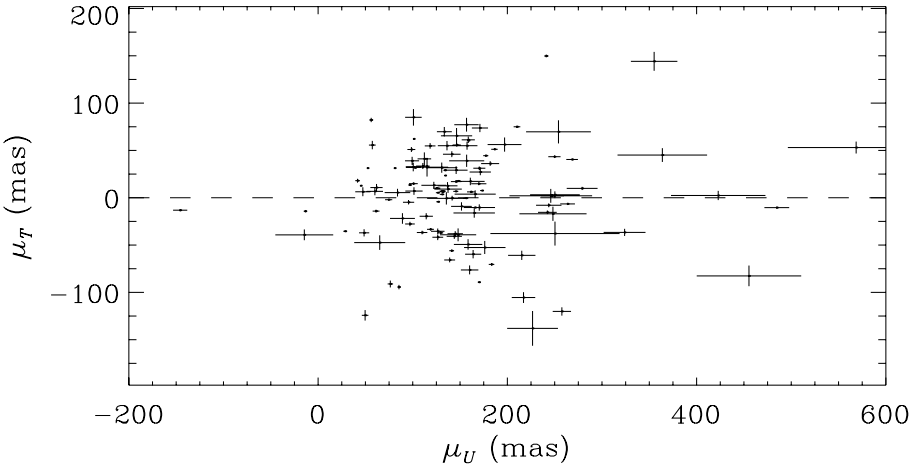

Fig. 6. Proper motion diagram (PMD) for single stars of the UMa flow (Sirius supercluster). The errorbars are calculated using the technique developed for the HIP catalogue (ESO, 1997) and are described in detail in Paper I.

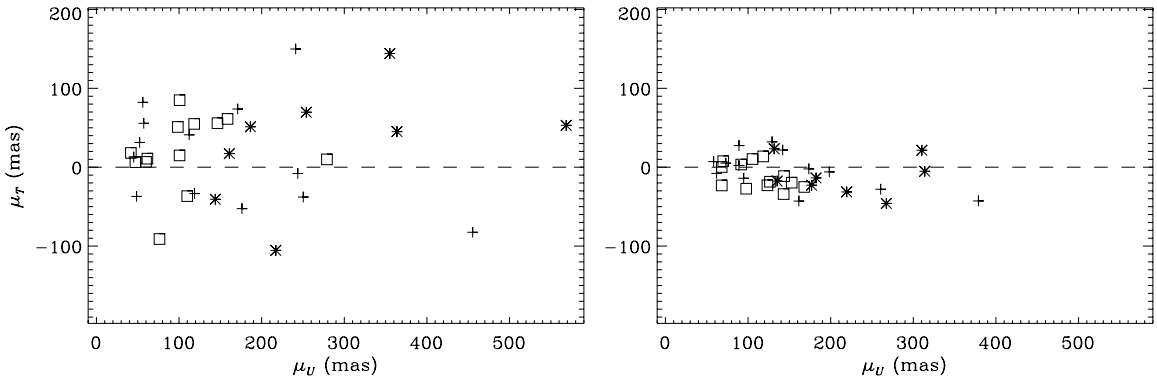

Fig. 7. The PMD for the stars belonging to the substructures in the UMa flow. The squares are the stars included in group 1, crosses – group 2, and asterisks – group 3.

Table 5. The mean μ_T and σ_{μ_T} of stars from Figs. 6 and 7.

	UMa stream apex		individual apex	
group	$\langle\mu_T\rangle$	σ_{μ_T}	$\langle\mu_T\rangle$	σ_{μ_T}
1	19.0	46.1	–11.3	16.2
2	15.0	65.3	–3.7	24.0
3	29.3	74.9	–11.5	24.2
nucleus	5.8	1.4	–0.5	1.1
corona	–1.8	45.2		

could include the analysis of μ_U-components. Since we consider their dependence on the angle λ, we use μ''_U that is not normalized to the geometrical center of the nucleus, but normalized to a unique R_c. Consider the dependence $\mu''_U - \sin\lambda$ in each of the hemispheres: $\cos\lambda > 0$ in PA (see above) and $\cos\lambda < 0$ in PaA. It should be a linear dependence: according to Fig. 5, μ'_U is proportional to $V\sin\lambda$, where V does not depend on λ. The dependence should be $\mu''_U = k\sin\lambda$. The coefficient k depends on the average weighted value of μ_U:

$$k = \frac{1}{\sin\lambda_c}\frac{\Sigma\mu_{U_i}\pi_i\sin\lambda_i}{\Sigma\pi_i\sin\lambda_i} = \frac{\langle\mu_U\rangle}{\sin\lambda_c} \quad (2)$$

and is defined for each of the hemispheres separately. $1/\sin\lambda_c$ is the normalization to the abovementioned large circle, and $\pi_i\sin\lambda_i$ are the weights. The lines constructed with the formula $\mu''_U = k\mathrm{sign}(\cos\lambda)\sin\lambda$ and appropriate stars from Table 7 are shown in Fig. 8a–d. In Fig. 9 the nucleus stars are shown. 5 stars are single objects with known radial velocity.

We analyse the plots in Figs. 8 and 9.

1. For the stars of the nucleus, the scatter of points in Fig. 9 is minimal; this suggests high accuracy of their motions to the apex.
2. In Fig. 8 we group the plots in pairs: to the left are hemispheres with the pole in the antapex (PaA), to the right are hemispheres with the pole in the apex (PA). The nucleus is located inside PA. The slopes of approximation lines for the corona (Fig. 8a) and group 1 (Fig. 8b) in the different hemispheres are very similar. This provides evidence for the movement of the stars of these structures located in the different hemispheres in the direction "antapex – apex". The location of the apexes of group 1 and corona slightly differs (as do the slopes of the lines). The lower set of plots shows a different picture. For the groups 2 (Fig. 8c) and 3 (Fig. 8d) the slopes of the lines in the plots for different hemispheres are different. This is evidence of the absence of coincidence of mean directions of motions of stars located in different hemispheres. This absence of coincidence may be a consequence of these systems being small.
3. The scatter of points relative to the straight lines of approximations is similar for the groups and corona (see Fig. 8). This confirms the kinematic similarity of their motion to the apex. The dispersion of peculiar velocities is similar in both cases.

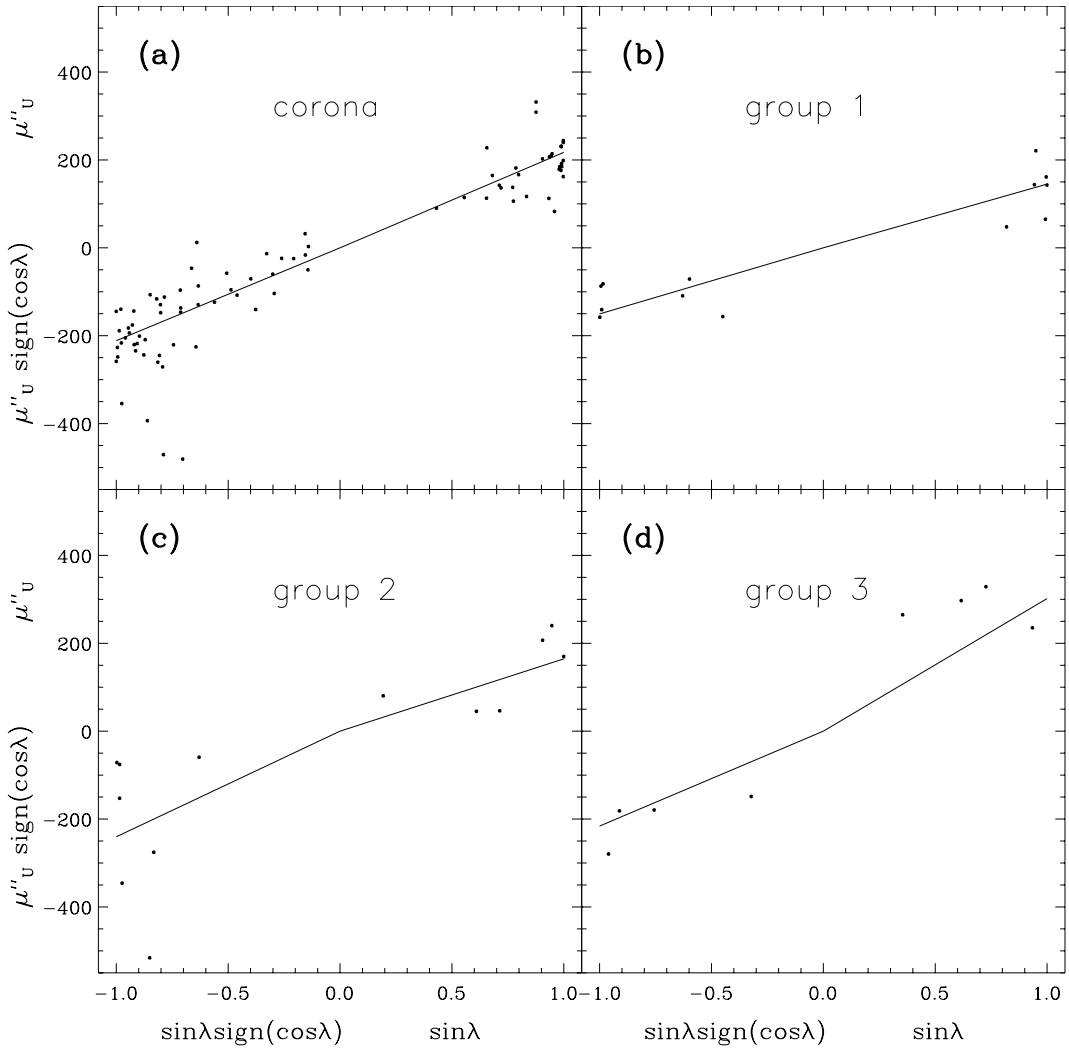

Fig. 8. Proper motion component μ''_U dependence on $\sin\lambda$ for UMa flow structures: **a)** corona, **b)** group 1, **c)** group 2 and **d)** group 3.

4. The slopes of straight lines for the nucleus (Fig. 9), corona (Fig. 8a) and groups (Fig. 8b–d) are different. This is evidence for the difference of the apexes of these structures.
5. Four stars to the left clearly are excluded from the dependence represented in Fig. 8a: HIP 5493, 29716, 63415, 67388. This is due to the overestimated μ_U value and the possible nonmembership of these stars (Table 7).
6. The star 60599 is excluded from Fig. 8c due to the overestimated μ_U value and possible nonmembership of group 2.

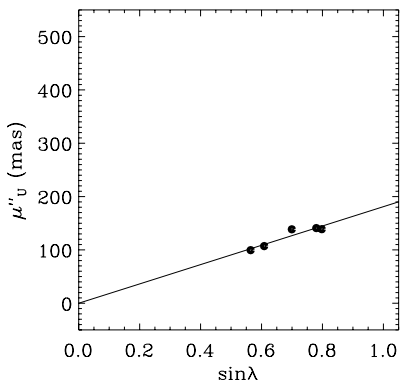

Fig. 9. Dependence $\mu''_U - \sin\lambda$ for the nucleus of the UMa stream.

6. Discussion

Table 7 contain all stars studied by us according to their membership of the nucleus, corona or groups.

As we noted above, we considered stars that were listed by different authors as probable members of the UMa flow. However for some of them one of the parameters of our diagrams deviates by more than 3σ, which requires revision of their membership of the flow.

The data on these stars are given in Table 7 as "possible non members" for group 2, group 3 and the corona. There are six such stars. For stars HIP 29716, 115669, 112211, 105928 the reason is an excess of V_r over the average, up to 30 km s^{-1}. Stars that have one parameter that deviates by more than 3σ from the regions are indicated in Figs. 1, 4 or 8. One of the reasons for this deviation may be significant errors of proper motions or radial velocity measurments. Because of this, definitive conclusions cannot be made. We consider them as possible nonmembers of the flow. From the values of the flags we conclude that all stars (excluding HIP 29716) were considered by Roman (1949) only. HIP 29716 was included in the flow by King et al. (2003) based on the measurements of the photometric index. The reason for the enhanced radial velocity of this star is unknown.

Table 6. The number of stars in substructures in the corona of UMa flow after taking into account the extremely high V_r and μ values.

Number	Number of stars	Final number of stars
1	13	13
2	13	12
3	8	5
Nucleus	8	8
Corona as a whole	86	76

For the stars that belong to the corona of the flow a large scatter of proper motions is typical. This is seen in Fig. 6: while all stars of the nucleus are located in a box $\Delta\mu_{\rm T}\times\Delta\mu_{\rm U}$ = 20×20 mas (see Paper I), for the flow the size of the box is 400 × 800 mas. This indicates large peculiar motions and the possible existence of subsystems in the corona. As we have seen above, inside separate groups, the scatter of proper motions reduces significantly with transition to the apexes of the groups (see Table 5). From Fig. 6, we see that some stars have greater $\mu_{\rm T}$ for a $3\sigma \approx 100$ interval ($\sigma_{\mu_{\rm T}}$ = 28.5): HIP 5493, 36827, 48331, 49544, 53907, 57548, 62103, 77163, 113829 and 115669; among them 36837, 48331, 62103, 77163 and 115669 are members of the groups. After transition to the group apex they shift in the direction of the μ_U-axis and are located within 3σ (see Fig. 7). Group 3 is the most concentrated and has the largest $\sigma_{\mu_{\rm T}}$, far higher than the rms for the corona (see Table 5). Thus group 3 may contain up to 3 stars less (i.e., its membership list may be reduced by more than 30%); this may cast doubt on its existence.

In Table 6 we summarize the data on the number of stars that belong to structures inside UMa flow. While corona stars are distributed approximately inside a sphere with a 150 pc radius, the groups have an elongated shape.

Now we check whether the stars in the groups discussed above belong to known kinematic groups.

We constructed the distributions of components of stellar spatial velocities shown in Fig. 10. We show in Fig. 10 the positions of known stellar streams taken from Montes et al. (2001). There is no overlap in the panels of Fig. 10 between their groups and ours. The space velocity vectors of the groups and stream have different directions. This confirms the absence of a kinematical relation between them. The kinematical segregation of the UMa corona groups is one of the results of the present study. This is in agreement with Eggen (1996) about the presence within superclusters (including Ursa Majoris itself) of independent local streams.

According to the classical approach (see e.g. Eggen 1998) the observed non-homogeneities in the velocity distribution are due to star formation non-uniformity. The observed picture does not contradict this point. In Fig. 10 the kinematical groups detected in the present study occupy positions different to those of known stream diagrams of spatial velocities. They represent small independent kinematical groups within the corona of the Ursa Majoris stream and include about 25% of the total corona population. This picture also does not conflict with present-day scenarios considering dynamic effects of redistribution of stellar orbits under the effect of spiral density waves or the Galactic central massive bar. In this case unevenness of the stellar velocity distribution can produce clumps in the velocity space in areas of already known streams, which are not genetically related to the streams. Such models were proposed by Famaey et al. (2005) and considered in detail by Quillen & Minchev (2005).

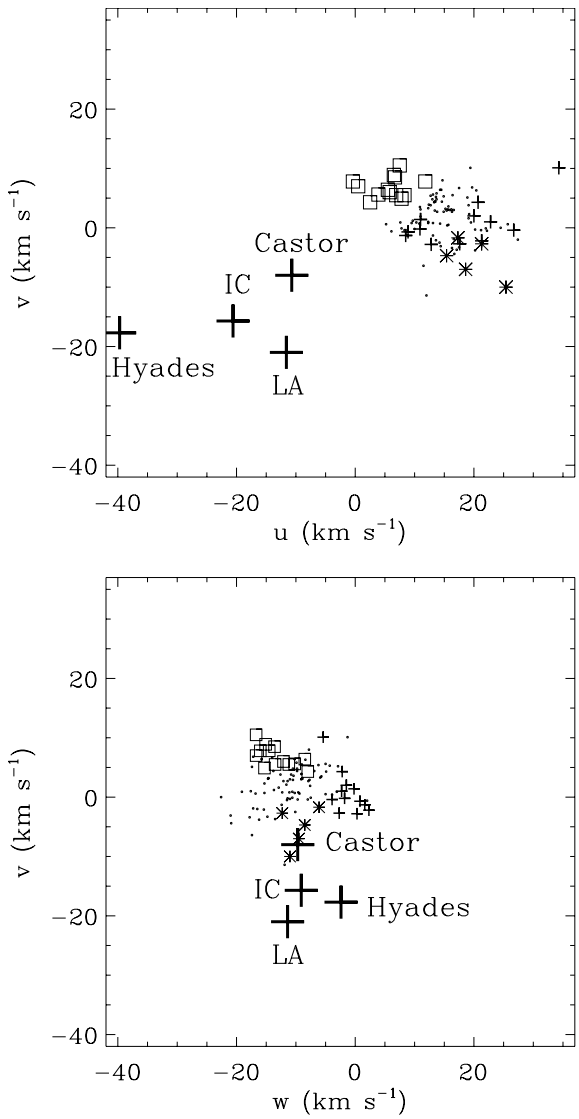

Fig. 10. (u, v) and (w, v) planes (Boetlinger Diagram) in the region of young disk stars. Large crosses are centered on the five young stellar kinematic groups analysed by Montes et al. (2001): Hyades, the Local Association (LA), Castor, IC 2391 (IC) and UMa. The squares label the stars indicated in group 1, crosses – group 2, asterisks – group 3, points – corona.

7. Conclusion

Our method of AD-diagrams (Paper I) is applied to the corona of the UMa flow (Sirius supercluster). The AD-diagram that includes all stars of the flow is inhomogeneous. Apart from the nucleus, several other regions of enhanced concentration of stars are seen in Fig. 1. By analysis of the parameters of the stars from these groups, we found common features in their kinematics. Thus, using diagrams of proper motion, we corrected the kinematics by transition to the individual (group) positions of apexes. This resulted in a significant reduction of the scatter of points in the diagrams and together with the analysis of radial velocities lead us to the conclusion that, other than the clear nucleus, three additional groups of stars exist in the corona, that contain 13, 13 and 8 stars, respectively. These groups have different directions of spatial motion and the locations of their apexes differ considerably from the mean apex for the flow as a whole. Some of these groups may have inner rotational components of motion inside

the flow. The corona, as an entity, has a unique component of motion "apex – antapex".

Our hypothesis of the existence of distinct groups of stars is not equally justified for all groups. Thus, after consideration of radial velocities and longitudinal components of proper motions, the number of stars in different groups was reduced (see Table 6). We can only speculate on the origin of sub-structures in the corona of the Sirius supercluster. They could be local streams in an evaporating cluster, linked genetically to the cluster or could be local inhomogeneities in the field star velocity space, super imposed on the cluster velocity distribution. In the latter case they are Galactic disk stars, which are not genetically connected to the cluster. The kinematical inhomogeneity of the UMa flow corona remains the main conclusion of the present study.

26% of stars previously considered as corona members actually comprise small, kinematically independent groups. Their status is not clear. They could be either stars genetically related to the corona that are evaporating from it, or field stars that have been cast into the UMa kinematical domain by dynamical effects related to spiral waves.

Acknowledgements. We thank L. R. Yungelson and A. E. Piskunov for reading the manuscript. The authors thank the referee for useful comments and suggestions.

References

van Altena, W. F. 1969, AJ, 74, 2
Chupina, N. V., Reva, V. G., & Vereshchagin, S. V. 2001, A&A, 371, 115 (Paper I)
Duflot, M., Figon, P., & Meyssonnier, N. 1995, A&AS, 114, 269
Eggen, O. J. 1959, MNRAS, 118, 65
Eggen, O. J. 1996, AJ, 112, 1595
Eggen, O. J. 1998, AJ, 116, 782
Famaey, B., Jorissen, A., Luri, X., et al. 2005, A&A, 430, 165
ESA 1997, The Hipparcos and Tycho catalogues, ESA SP-1200
King, J. R., Villarreal, A. R., Soderblom, D. R., Gulliver, A. F., & Adelman, S. J. 2003, AJ, 125, 1980
Montes, D., Lopez-Santiago, J., Galvez, M. C., et al. 2001, MNRAS, 328, 45
Quillen, A. C., & Minchev, I. 2005, AJ, 130, 576
Roman, N. G. 1949, ApJ, 110, 205
Soderblom, D. R., & Mayor, M. 1993, AJ, 105, 226

Online Material

Table 7. List of stars according to their membership in the nucleus, corona or groups. Observational data on the stars with non-zero membership probability according to published data (R – according to Roman (1949), E_1 – Eggen (1959), S – Soderblom & Major (1993), E_2 – Eggen (1998), M – Montes et al. (2001), K – King et al. (2003)).

HIP	HD	μ_α mas/yr	σ_{μ_α}	μ_δ mas/yr	σ_{μ_δ}	π mas	σ_π	V_r km s^{-1}	μ_U mas/yr	σ_{μ_U}	μ_T mas/yr	σ_{μ_T}	$\sin\lambda$	R	E_1	S	E_2	M	K
nucleus																			
51814	91480	65.65	0.45	37.11	0.38	37.80	0.61	–10.4	130.99	2.37	3.62	0.55	0.5394	1	1	1	1	1	1
53910	95418	81.66	0.37	33.74	0.38	41.07	0.60	–12.0	130.28	2.09	6.92	0.46	0.5841	1	1	1	1	0	1
58001	103287	107.76	0.48	11.16	0.50	38.99	0.68	–12.6	145.48	2.65	6.76	0.65	0.6761	1	1	1	1	0	1
61946	110463	121.53	0.65	–4.36	0.63	43.06	0.82	–6.3	131.64	2.57	6.33	0.75	0.7596	1	1	1	0	1	1
62956	112185	111.74	0.45	–8.99	0.49	40.30	0.62	–9.3	126.55	2.10	5.41	0.62	0.7785	1	1	1	1	0	1
group 1																			
4520	5612	–5.97	0.73	–5.76	0.55	6.24	0.82	15.2	47.23	8.04	6.38	4.70	0.9929	1	0	0	0	0	0
7906	10348	–8.10	0.80	–6.50	0.48	6.23	0.80	5.2	60.00	8.61	6.79	4.09	0.9814	1	0	0	0	0	0
8588	11257	–69.33	0.83	–27.84	0.79	23.46	1.02	11.1	109.90	5.58	–36.68	1.87	0.9994	1	0	0	0	0	1
29884	43244	–43.79	0.64	11.26	0.38	13.86	0.78	–8.0	279.02	16.32	9.90	1.67	0.4136	1	0	0	0	0	1
35628	56168	–70.56	0.59	70.11	0.92	39.10	1.15	–8.9	146.47	4.31	55.80	1.86	0.5532	0	0	0	0	1	1
36827	60491	–83.68	1.56	–43.15	0.81	40.32	1.26	–9.7	76.33	2.90	–91.07	3.62	0.6785	0	0	0	0	1	1
64078	114038	16.03	1.03	–9.38	0.69	10.66	0.84	–9.1	61.69	6.47	10.84	3.80	0.9932	1	0	0	0	0	0
66200	118022	43.89	0.65	–24.03	0.60	17.79	0.80	–11.9	100.62	4.67	14.93	1.46	0.9851	1	1	0	0	0	1
71759	129153	53.76	0.76	–14.71	0.64	18.83	0.85	–7.9	98.54	4.21	51.01	2.62	0.9994	0	1	0	0	0	0
75342	137006	76.73	0.85	–28.21	0.72	18.20	0.78	–2.2	158.70	6.91	61.23	3.34	0.9651	1	0	0	0	0	1
77163	140775	27.17	0.77	–3.19	0.70	8.49	0.73	–9.8	100.71	8.79	84.99	8.73	0.9633	1	0	0	0	0	1
109577	210702	–2.94	0.71	–18.79	0.65	17.88	0.74	10.9	41.68	2.48	18.04	2.03	0.8509	1	0	0	0	0	0
116354	221756	–17.71	0.45	–45.77	0.42	13.97	0.63	13.0	118.33	5.65	54.84	2.92	0.9996	1	0	0	0	0	1
group 2																			
954	745	–32.99	0.84	–18.32	0.61	7.81	0.96	–1.8	176.14	21.92	–52.54	6.88	0.9489	0	0	0	0	1	1
1473	1404	–66.51	0.57	–42.48	0.43	23.11	0.68	–8.0	118.74	3.65	–33.38	1.23	0.9996	1	1	0	0	0	1
3231	3817	–14.37	0.66	–3.02	0.69	9.47	0.81	–5.1	48.62	5.41	–37.03	3.77	0.9930	1	0	0	0	0	0
13244	18293	–33.95	0.42	–27.18	0.51	9.92	0.48	4.7	171.01	8.55	73.74	4.33	0.8556	0	1	0	0	0	0
13717	18331	–35.75	2.53	–43.31	1.35	17.28	0.93	–15.0	112.26	7.20	41.08	6.88	0.9927	1	0	0	0	0	1
38747	64942	21.01	1.08	–25.39	0.95	20.69	1.15	–8.1	57.24	3.59	55.67	4.47	0.7053	0	0	0	0	1	1
48331	85512	461.28	0.66	–472.87	0.66	89.67	0.82	–9.6	241.12	2.23	149.86	1.48	0.9892	0	0	0	0	1	1
59152		120.06	1.54	–73.58	0.72	25.27	1.40	–5.5	243.74	13.43	–7.94	2.02	0.8099	0	0	0	0	1	1
59199	105452	100.18	0.69	–39.33	0.55	67.71	0.75	4.4	52.30	0.68	31.39	0.51	0.9896	1	1	0	0	0	0
80337	147513	72.64	0.84	3.41	0.65	77.69	0.86	10.1	45.12	0.85	12.81	0.40	0.7071	0	0	1	0	1	0
102395	197051	–42.40	0.46	10.57	0.46	23.71	0.63	9.8	56.11	2.05	82.24	2.30	0.5252	0	1	0	0	0	0
102978	198542	–7.97	1.05	–2.54	0.83	5.19	0.95	9.0	250.32	68.29	–37.81	12.67	0.2015	1	0	0	0	0	0
possible non members of group 2																			
60599	108123	56.82	0.92	–41.09	0.55	6.56	0.79	–5.3	455.35	55.20	–82.53	10.95	0.8220	1	0	0	0	0	0
group 3																			
3909	4813	–224.67	0.96	–228.44	0.63	64.69	1.03	7.7	186.37	3.39	51.27	0.90	0.9215	1	0	0	0	0	1
36425	59294	1.26	0.74	–19.26	0.47	5.82	0.79	–15.4	254.02	34.27	69.67	12.21	0.4199	0	1	0	0	0	0
50061	88654	23.44	0.97	–30.88	0.69	10.80	0.96	–7.0	160.90	15.07	17.29	3.99	0.7870	0	0	0	0	1	1
56154	100043	30.16	0.66	–51.37	0.61	15.56	0.82	–1.8	143.91	8.00	–40.67	2.79	0.9213	0	0	0	0	1	1
62103	110646	48.10	0.68	–74.58	0.45	14.26	0.77	0.7	217.08	12.38	–105.44	5.74	0.9559	1	0	0	0	0	0
possible non members of group 3																			
105928	204139	–24.64	0.85	–33.95	0.46	7.05	0.84	23.0	568.60	72.23	53.04	6.30	0.3649	1	0	0	0	0	0
112211	215167	–31.40	0.92	–28.02	0.62	6.73	0.85	21.6	363.75	47.32	45.16	7.27	0.6029	1	0	0	0	0	0
115669	220704	–50.13	0.77	–62.97	0.69	10.57	0.72	15.7	355.13	24.58	144.17	9.98	0.7034	1	0	0	0	0	0
the other corona stars																			
2213	2410	–22.30	0.72	–17.33	0.49	6.12	0.79	8.3	164.99	21.90	–16.02	5.02	0.9889	0	0	0	0	1	1
3245	3919	–28.92	0.59	1.04	0.47	13.19	0.67	18.8	97.09	5.12	–27.66	2.26	0.7750	0	1	0	0	0	0
5121	6482	–30.48	0.63	–34.24	0.51	10.58	0.72	12.3	157.39	10.93	54.99	4.24	0.9437	1	0	0	0	0	0
6061	7804	–48.38	0.85	–22.37	0.62	14.83	0.86	5.3	126.45	7.09	–35.41	2.93	0.9876	1	0	0	0	0	1
12647	16861	–24.27	1.04	–23.37	0.88	7.66	0.94	6.1	156.99	18.56	39.10	6.50	0.9772	1	0	0	0	0	1
14146	18978	–145.96	0.54	–55.76	0.55	37.85	0.69	–9.8	141.14	2.56	–55.93	1.34	0.9978	1	0	0	0	0	0
17874	24160	–49.42	0.47	–56.63	0.60	15.54	0.58	2.0	170.35	6.38	31.21	1.88	0.9979	0	1	1	0	1	1
20266	27022	–28.52	0.44	–4.70	0.52	9.80	0.67	–18.5	136.19	9.66	55.09	4.97	0.7120	1	0	0	0	0	0
20507	27861	–47.92	0.81	–56.73	0.80	15.66	0.80	–11.0	181.81	9.50	36.17	2.48	0.9136	1	1	0	1	0	1

Table 7. continued.

HIP	HD	μ_α mas/yr	σ_{μ_α}	μ_δ mas/yr	σ_{μ_δ}	π mas	σ_π	V_r km s^{-1}	$\mu_{\rm U}$ mas/yr	$\sigma_{\mu_{\rm U}}$	$\mu_{\rm T}$ mas/yr	$\sigma_{\mu_{\rm T}}$	$\sin\lambda$	R	E_1	S	E_2	M	K
21295	28978	–15.58	1.21	–7.77	1.03	7.99	1.09	–7.6	89.17	13.15	–21.82	5.59	0.8485	1	0	0	0	0	0
22678	30834	–25.97	0.94	–3.89	0.78	5.81	0.82	–16.5	248.19	35.47	–16.96	7.50	0.6436	1	1	0	0	0	1
22776	31000	6.17	1.02	11.58	0.85	35.14	1.12	–6.2	–13.48	1.79	–14.16	1.27	0.6400	0	0	0	0	1	1
27015	34109	–10.52	0.49	11.39	0.61	6.90	0.56	–14.0	101.27	9.14	7.11	3.98	0.7848	0	0	0	1	0	0
28954	41593	–122.30	0.89	–103.29	0.57	64.71	0.91	–11.7	156.28	2.55	–0.42	0.45	0.5610	0	0	1	0	1	1
29295	42581	–137.01	0.61	–714.06	0.89	173.19	1.12	4.3	158.96	1.08	60.49	0.50	0.8963	0	0	0	0	0	1
29789	43261	–13.64	0.87	–8.59	0.57	7.48	0.84	–20.9	165.98	21.73	3.81	4.04	0.4599	1	0	0	0	0	0
33277	50692	–35.75	1.01	25.14	0.59	57.89	0.90	–14.7	28.63	1.97	–35.35	0.80	0.3275	0	0	0	0	0	1
33485	50973	–21.67	0.85	–3.18	0.51	14.49	0.69	–8.0	141.27	9.29	46.05	3.08	0.3007	1	0	0	0	0	1
36704	59747	–50.10	2.03	8.54	0.90	50.80	1.29	–18.4	247.61	12.33	2.18	1.13	0.1431	0	0	0	0	1	1
38228	63433	–9.29	0.99	–11.84	0.71	45.84	0.89	–18.7	74.54	3.80	–2.02	1.0	0.1549	0	0	0	0	1	1
39095	65810	–7.29	0.85	–35.07	0.93	13.69	0.81	–12.0	114.27	7.01	–19.50	3.29	0.8025	1	1	0	1	0	0
42438	72905	–27.73	0.59	87.90	0.49	70.07	0.71	–12.0	80.98	0.96	31.34	0.56	0.5061	1	0	1	0	1	1
42954	74485	–3.27	0.88	–4.26	0.54	6.84	0.76	–12.2	–14.60	30.60	–39.15	5.75	0.1411	1	0	0	0	0	0
43670	75935	10.51	2.20	–6.53	1.14	24.66	1.34	–19.0	83.86	13.49	5.44	4.04	0.2070	0	0	0	0	1	1
43852	76218	–23.50	1.19	–12.23	0.86	38.21	1.00	–12.8	–145.78	7.53	–13.16	1.17	0.1559	0	0	0	0	1	1
44382	78045	–2.01	0.57	–95.80	0.44	26.24	0.51	4.9	129.45	2.68	–36.98	1.18	0.9791	0	1	0	1	0	0
44405	77350	–2.56	1.05	–7.13	0.96	7.14	0.96	–14.3	65.11	26.91	–47.34	7.72	0.2606	1	1	0	0	0	1
45493	79439	49.14	0.98	59.79	0.54	27.55	0.80	–18.7	263.66	7.74	–6.48	1.15	0.3772	1	0	0	0	0	1
45590	79763	14.11	0.68	11.91	0.49	8.89	0.85	–13.1	250.26	26.26	3.19	3.61	0.2940	0	1	0	0	0	0
46324	81659	37.60	1.08	–130.77	0.67	25.07	1.00	–16.8	242.26	9.89	–15.34	1.93	0.7927	0	0	0	0	1	1
48341	85364	13.76	0.94	–28.25	0.55	16.31	0.80	–10.0	95.58	5.90	–4.69	2.35	0.7135	0	0	1	0	0	1
48356	85444	18.68	0.95	–21.88	0.55	11.92	0.81	–14.5	100.52	7.99	32.57	4.54	0.8194	1	0	1	0	1	1
49593	87696	50.97	0.69	0.64	0.52	35.78	0.84	–17.6	125.40	3.74	10.23	0.79	0.3985	1	1	0	1	0	1
51914	91752	36.92	0.67	–33.84	0.41	21.60	0.75	–23.7	139.01	5.74	–65.68	2.58	0.4871	0	0	0	0	0	1
53985	95650	141.43	1.45	–51.13	0.99	85.76	1.36	–14.9	96.98	1.81	13.52	0.62	0.6332	0	0	0	0	1	1
56337	100310	59.35	0.99	–10.57	0.73	22.33	1.22	–9.6	144.89	8.11	–37.99	2.75	0.6337	0	0	0	0	1	1
59496	238087	101.96	0.97	20.26	1.01	35.24	1.24	–15.0	145.78	5.49	17.16	1.62	0.7123	0	0	0	0	1	1
61748	110066	19.31	0.67	–2.63	0.53	6.45	0.73	–14.8	130.60	16.58	31.80	5.39	0.8016	0	0	0	1	0	0
62541	111397	28.96	0.82	–20.23	0.51	8.10	0.77	–8.1	170.36	16.59	–10.27	3.39	0.9063	1	1	0	1	0	1
62933	112097	63.35	0.73	–35.13	0.47	16.40	0.78	–10.0	169.77	8.06	14.88	1.63	0.9200	1	1	0	0	0	0
64626	238208	82.45	1.13	–36.65	1.13	17.87	1.19		215.24	14.48	–60.80	4.87	0.8069	0	0	0	0	0	1
67057	119605	12.62	0.88	–5.63	0.81	4.18	0.72	0.7	115.14	22.23	32.32	9.93	0.9979	1	0	0	0	0	0
67596	120818	32.16	0.58	–8.29	0.47	11.24	0.68	–12.3	110.68	7.11	33.54	3.21	0.9215	1	1	0	0	0	1
70029	125642	26.72	0.47	–10.18	0.52	7.30	0.60	–10.5	145.82	12.08	29.22	4.09	0.9414	1	1	0	0	0	1
71395	128311	205.46	0.89	–249.68	0.70	60.35	0.99	–9.6	183.24	2.94	–70.38	1.40	0.9999	0	0	0	0	1	1
72944		275.95	1.95	–122.11	1.33	101.91	1.67	+05.	102.52	1.76	31.73	0.93	0.9999	0	0	0	0	1	0
74702	135599	178.02	0.85	–136.52	0.70	64.19	0.97	–3.1	126.86	1.95	–4.24	0.53	0.9761	0	0	0	0	0	1
75973	138481	11.02	0.52	–8.81	0.51	3.74	0.54	–10.4	135.56	20.33	–0.64	6.51	0.9863	1	0	0	0	0	1
76330	139194	119.37	0.78	–93.23	0.87	33.37	0.88	–14.0	161.66	4.22	6.25	1.24	0.9947	0	0	0	0	1	1
76810	140027	22.16	0.71	–16.80	0.85	7.24	0.79	3.4	137.32	14.52	9.17	4.03	0.9902	1	1	0	0	0	0
77578	141680	30.15	0.71	–47.62	0.63	12.40	0.73	–3.5	160.08	9.25	–76.21	4.76	0.9481	1	0	0	0	0	0
79945	146834	16.84	0.94	–15.31	0.74	6.65	0.84	8.0	147.92	19.13	–39.13	6.81	0.7983	1	0	0	0	0	0
80459		432.29	1.32	–170.71	1.21	151.93	1.11		101.12	0.79	62.24	0.64	0.9794	0	0	0	0	1	0
80686	147584	199.89	0.31	110.77	0.51	82.61	0.57	7.6	134.24	0.97	23.48	0.32	0.7198	0	1	1	0	0	1
81800	151044	133.43	0.51	–107.77	0.48	34.00	0.50		177.18	2.71	44.53	1.11	0.9933	1	0	0	0	0	1
85185	157740	12.58	0.46	–28.83	0.50	7.55	0.71	11.2	158.49	15.01	–49.35	5.55	0.9051	0	1	0	0	0	0
88694	165185	105.44	0.98	7.99	0.56	57.58	0.77	13.2	148.07	2.67	17.75	0.48	0.4313	0	0	1	1	1	1
89282	167389	51.47	0.55	–128.53	0.58	29.91	0.59	–3.0	165.89	3.41	–10.24	0.94	0.9880	0	0	0	0	1	1
90182	172864	18.39	0.53	–23.40	0.52	5.95	0.52	–11.2	197.03	17.85	56.25	7.46	0.8767	0	0	0	1	0	0
90342	169981	23.23	0.54	–24.45	0.51	7.63	0.60	7.5	156.81	12.90	77.23	7.25	0.9360	1	1	0	0	0	1
91322	171978	11.74	1.05	–19.83	0.81	5.06	0.93	11.4	245.87	43.74	2.06	7.33	0.6565	1	1	0	0	0	0
92919	175742	130.79	0.59	–283.07	0.74	46.64	1.03	10.3	268.44	6.15	40.53	1.13	0.8762	0	0	0	0	0	1
93179	176232	0.94	0.72	–51.42	0.58	13.45	0.67	14.5	163.82	8.54	–59.58	4.44	0.7860	0	1	0	0	0	0
94083	180777	51.63	0.62	–119.80	0.46	36.64	0.49	–4.0	134.16	1.81	29.09	0.94	0.9279	1	1	1	1	0	1
95352	182694	16.30	0.41	–27.36	0.46	8.06	0.47	–0.1	133.42	7.84	69.87	4.97	0.9818	0	1	0	0	0	0
96258	184960	31.72	0.47	–188.14	0.50	39.08	0.47	0.4	173.27	2.08	7.61	0.61	0.9982	1	1	0	1	1	1
102281	197461	–19.61	0.71	–41.74	0.51	16.03	0.68	9.3	126.44	5.72	–41.75	3.02	0.7717	0	1	0	0	0	0
106481	205435	–24.48	0.51	–93.88	0.45	26.20	0.51	6.9	132.26	2.62	7.00	1.0	0.9916	1	0	0	0	1	1

Table 7. continued.

HIP	HD	μ_α mas/yr	σ_{μ_α}	μ_δ mas/yr	σ_{μ_δ}	π mas	σ_π	V_r km s^{-1}	μ_U mas/yr	σ_{μ_U}	μ_T mas/yr	σ_{μ_T}	$\sin\lambda$	R	E_1	S	E_2	M	K
107555	207636	–10.46	0.55	–25.07	0.44	6.62	0.47	–2.0	151.47	10.97	–9.14	4.35	0.9591	0	0	0	1	0	0
108991	209625	–20.05	1.13	–42.57	0.55	14.10	0.82	18.9	171.37	11.26	27.22	3.32	0.6809	1	1	0	0	0	0
109410	210459	–12.34	0.42	–17.94	0.58	12.96	0.62	2.0	61.24	3.61	–14.09	1.52	0.9585	1	1	0	0	0	1
109434	210873	–8.49	0.49	–21.74	0.40	6.38	0.48	–2.8	136.77	10.51	12.60	3.97	0.9457	1	0	0	1	0	1
110091	211575	–41.39	1.37	–54.73	0.58	24.11	0.92	15.0	141.66	6.32	–0.38	2.52	0.7120	0	0	0	0	1	1
113774	217595	–22.06	1.02	–11.21	0.73	9.37	0.90		146.32	16.50	65.53	8.20	0.5553	0	1	0	0	0	0
115312	220096	–19.59	0.89	–11.20	0.82	9.92	0.87	13.9	122.29	13.13	13.17	3.71	0.6548	0	0	0	0	0	1
116928	222603	–129.55	0.77	–154.87	0.63	32.38	0.84	12.4	249.77	6.46	43.42	1.41	0.8762	1	0	0	0	0	1
possible non members of corona																			
5493	6920	–135.76	0.53	–41.87	0.38	18.98	0.71	13.2	257.61	9.71	–120.10	4.37	0.9753	0	0	0	0	0	1
21818	29697	–233.61	1.03	–254.55	0.73	74.13	1.24	+11.	210.16	3.51	75.01	1.28	0.7442	0	0	0	0	1	0
29716	43318	–158.04	0.69	–218.33	0.51	28.02	0.76	38.1	484.75	13.07	–10.39	1.16	0.7031	0	0	0	0	0	1
49544		–64.84	1.96	–99.51	1.41	44.77	1.96	–20.	49.69	3.45	–124.23	5.55	0.6633	0	0	0	0	1	0
53907	95578	9.58	0.88	–36.11	0.63	6.34	0.78	–13.5	226.63	26.89	–137.95	18.37	0.8143	0	1	0	0	0	0
57548		605.62	2.14	–1219.23	1.86	299.58	2.20	–13.	170.10	1.36	–89.22	0.70	0.8707	0	0	0	0	1	0
63415	238179	97.73	1.22	–14.80	1.02	10.50	1.24		422.86	49.90	2.45	4.91	0.7890	1	0	0	0	0	1
67388	120528	98.24	0.85	–43.55	0.76	13.60	0.93		323.89	22.12	–36.57	3.80	0.8609	1	0	0	0	0	1
99913	192836	8.10	0.71	–25.73	0.61	10.95	0.75	–4.1	99.31	7.46	39.03	4.27	0.8338	1	0	0	0	0	0
113829	217813	–117.66	0.88	–28.13	0.66	41.19	0.87	0.0	85.47	1.84	–94.33	2.34	0.9334	0	0	0	0	1	1
not considered stars with $\sigma_\pi/\pi > 20\%$																			
7617	9900	2.98	0.50	–5.54	0.61	2.86	0.70	–8.1						1	0	0	0	0	0
10820	14274	–8.56	1.15	1.08	1.01	3.41	1.10							0	0	0	0	1	0
36041	58367	–2.95	0.81	–8.65	0.53	3.30	0.88	–7.9						1	0	0	0	0	0